Analysis of the performance of a refrigerated display cabinet fitted with a thermosiphon thermal accumulator for demand-side management

Maria Aurely Yedmel, Anthony Delahaye, Denis Leducq

Energy Conversion and Management 346 (2025) 120483

Contents lists available at ScienceDirect

Energy Conversion and Management

journal homepage: www.elsevier.com/locate/enconman

Analysis of the performance of a refrigerated display cabinet fitted with a thermosiphon thermal accumulator for demand-side management

Maria Aurely Yedmel *, Anthony Delahaye, Denis Leducq

Université Paris-Saclay, INRAE, FRISE, Antony 92761, France

ARTICLE INFO

Keywords:
Refrigeration
Thermosiphon
Thermal Energy Storage
PCM
Demand-side management
Power outages
Display cabinet

ABSTRACT

Demand-side management (DSM) is a key strategy for regulating electricity demand, especially in grids incorporating renewable energy sources. Like electrical batteries, thermal energy storage acts as a flexible load to alleviate grid stress. Therefore, to support demand response programs, an innovative Thermosiphon Thermal Accumulator (TTA) has been developed and integrated into vapour compression refrigeration systems to store and supply cold energy to the evaporator during power cuts. This article examines the performance of the TTA, integrated into a closed-door refrigerated display cabinet, during a 1.5-hour DSM event under varying operating conditions, using five key performance indicators. The results show that the accumulator successfully supplied cold energy to the evaporator during power cuts, while also mitigating product temperature rise during DSM event, ensuring compliance with regulatory temperature limits under all tested conditions. For all experiments, energy consumption during DSM with accumulator discharge was comparable to regular operation, with even a slight reduction (up to 7 % lower in some cases). This decrease in energy consumption is attributed to the lasting impact of DSM-related savings, which outweigh the short-term rebound effect. Experiments involving high thermal loads required up to 8 h to recharge the accumulator after DSM due to defrosting cycles. Interactions between door openings, defrost cycles, and thermostat settings were observed in some cases. With an ambient temperature of 19 °C, a thermostat setting of −1 °C, and 50 % product occupancy, the TTA can sustain two to three 1.5-hour DSM events in 24 h.

1. Introduction

Refrigerated Display Cabinets (RDCs) can be horizontal, vertical, or combined; plug-in or remote; opened- or closed-door; and operate with positive or negative cold storage. Widely used in supermarkets, they store chilled and frozen products at controlled temperatures while displaying them for sale. In 2021, RDCs accounted for 50.4 % of the global commercial refrigeration market, with the highest sales growth in Europe (+16.3 %) [1]. This upward trend is expected to continue, reaching a Compound Annual Growth Rate (CAGR) of 2.5 % between 2023 and 2032 [2]. Despite their growing market share, RDCs are major energy consumers, accounting for 30–60 % of a supermarket's electricity use [3], mainly due to their continuous 24/7 operation to maintain food safety.

With the growing threat of global warming, efficient energy management has become crucial. Governments worldwide are enforcing strict regulations to tackle energy consumption. For businesses, compliance is not only a legal duty but a strategic advantage. Supermarkets, like other sectors, are adopting innovative energy strategies, with demand-side management (DSM) emerging as a key solution. DSM is a set of measures to encourage household and industrial consumers to control their energy consumption patterns. It helps grid operators balance supply and demand in real time, prevent overloads, and support renewable energy integration by adding flexibility during production fluctuations.

To support DSM implementation in supermarkets, researchers have introduced numerous innovations to optimise refrigerated display cabinets (RDCs). Benefits extend beyond energy savings to improved temperature uniformity and reduced temperature rise during compressor cycling, defrosting, and power outages. Alzuwaid et al. [4] integrated water-gel PCM heat exchangers into the rear duct of an open RDC, achieving about 5 % energy savings and better temperature stability under climate class 3. Similarly, Ben-Abdallah et al. [5] and Ben-Abdallah et al. [6] demonstrated that integrating PCM into the rear duct of an open RDC enhances DSM flexibility by limiting product temperature rise during compressor shutdown – approximately 1 °C after 2 h, compared to 2 °C without PCM. Rivera and Moraga [7]

* Corresponding author.
E-mail address: maria-aurely.yedmel@inrae.fr (M.A. Yedmel).

https://doi.org/10.1016/j.enconman.2025.120483
Received 19 May 2025; Received in revised form 1 September 2025; Accepted 4 September 2025
Available online 17 September 2025

Nomenclature

Δh	Specific enthalpy kJ/kg
Δt	Time difference h
%	Percentage %
E	Energy consumption kWh
η	Efficiency /
Θ	Temperature°C
T	Time h

SUBSCRIPTS

Av	average
Ex	exergy
max	maximum
norm	normalised

ABBREVIATION

COP	Coefficient of Performance
CAGR	Compound Annual Growth Rate
DSM	Demand-Side Management
KPI	Key Performance Indicator
PCM	Phase Change Material
RT-4	Rubitherm RT −4
RT0	Rubitherm RT 0
RDC	Refrigerated Display Cabinet
SP	Solid Portion
TTA	Thermosiphon Thermal Accumulator
TXV	Thermostatic Expansion Valve
VCS	Vapour Compression System

showed that PCM plates in a domestic freezer's internal walls extended food freezing/defrosting periods and improved energy efficiency by 11.4 %. Purohit and Dasgupta [8] evaluated the benefits of PCM in display cabinets against initial and operating costs. They found that PCM lowers energy bills, preserves food shelf life, and shortens payback periods as electricity tariffs rise and food waste declines, enhancing operational sustainability. Rocha et al. [9] highlighted, in a review on latent energy potential, that most energy savings from PCM in refrigeration systems result from improved coefficient of performance (COP) and reduced compressor runtime. These savings are highly dependent on PCM placement within the equipment [10]. Javeri-Shahreza et al. [11] developed a dynamic model of a double open-display cabinet to assess PCM placement in the cabinet and on evaporator walls. PCM reduced temperature fluctuations, compressor cycles, and energy use by 15.8 %, 5.0 %, and 1.1 % in the cabinet, and by 6.6 %, 10.0 %, and 1.5 % in the evaporators. Yilmaz et al. [12] confirmed that PCM location within RDCs influences energy savings, with shelf placement yielding a 4.4 % reduction in energy use and more uniform air temperature compared to rear-duct positioning or no PCM.

These studies collectively confirm the benefits of incorporating PCM into refrigerated chambers and evaporator walls. To enhance these advantages without additional electricity use, researchers have combined PCM with thermosiphon technology. This approach enables precise temperature regulation in RDCs while helping to smooth energy demand peaks [13–16]. For instance, Dhumane et al. [13] designed a personal air conditioning system using PCM and thermosiphon, achieving a 24 % increase in COP. Liu et al. [15] introduced a cool-storage refrigerator with a controllable loop thermosiphon capable of improving temperature control accuracy from 2.1 °C to 0.6 °C. Yuan et al. [16] explored the energy-saving potential of natural cold source RDCs, maintaining package temperatures within preservation ranges and achieving up to a 41.95 % reduction in energy consumption.

Despite the growing interest in combining PCM and thermosiphon technologies, to the best of the authors' knowledge, no studies explored their application in closed refrigerated display cabinets to address demand-side management challenges. To this end, after evaluating the advantages and limitations of various PCM placements (shelves, air ducts, evaporators, and products), an innovative thermal energy storage device – referred to as the Thermosiphon Thermal Accumulator (TTA) – was introduced for the first time to enhance cooling performance in a closed refrigerated display cabinet during demand-side management events [17,18]. The TTA, composed of a finned-tube heat exchanger, PCM, and thermosiphon circulation pipes, was installed at the rear of the cabinet and directly incorporated into its vapour compression system (VCS). The new system design shows promise as a transformative solution, as it can be seamlessly integrated into any vapour compression system without requiring secondary fluids, additional cooling systems, or causing airflow obstructions within the cabinet. The Thermosiphon Thermal Accumulator was evaluated under a single, controlled operating condition – ambient temperature of 17 °C, thermostat set to −3 °C, with the display cabinet doors remaining closed throughout the test. The results were compelling: the accumulator effectively provided cold energy to the refrigerated display cabinet during a 1.5-hour DSM event, reducing air and product temperature increases by 3.2 °C and 0.9 °C, respectively [17]. Although significant temperature reductions were achieved in the previous work, no definitive conclusions could be drawn regarding the TTA's suitability for demand-side management, as its performance under various conditions, energy consumption, and economic viability were not investigated – factors that are critical for validating the efficiency of any system. The current study directly addresses this gap by evaluating the performance of the TTA during a 1.5-hour DSM event – consistent with the previous work – but under a range of ambient and thermostat temperatures, two standardised door-opening scenarios, three different cabinet product loads, and two types of PCMs. Energy consumption and thermal stability across all scenarios were evaluated using key performance indicators (KPIs). A cost-benefit analysis was also performed. The experimental results and related calculations are presented and critically discussed in this paper.

2. Materials and methods

2.1. Materials

This study evaluates the performance of a refrigerated display cabinet equipped with a thermosiphon thermal accumulator for demand-side management applications. Detailed descriptions of the refrigerated display cabinet specifications, thermal accumulator design, and associated instrumentation are provided to ensure the reproducibility of the experimental setup and results.

2.1.1. Refrigerated display cabinet

A commercial vertical refrigerated display cabinet (OFFLIP 2 Eco DV; 200 × 134.5 × 70.5 cm; 230 V – 50 Hz) was used to evaluate the performance of the thermosiphon thermal accumulator (TTA). This cabinet is a closed-door plug-in type designed for positive cold storage (0/2 °C) and operates with R404A refrigerant. It meets the specifications for cabinet class M1 and climate class 3. The cabinet features five shelves, each with six rows of products of different heights. Methylcellulose packages (20 × 10 × 5 cm) were used to simulate food products. The air inside the cabinet is cooled by an evaporator beneath the bottom shelf. From there, the cold air moves upward through a vertical duct at the back. Some airflow is directed into the shelves to cool the products, while the rest flows to a discharge grid. There, an air curtain is created to protect the front products. The air curtain mixes with the air from the

shelves and flows downward to a return air grid, where it is cooled again before being circulated back into the cabinet. The TTA was positioned outside the cabinet and mounted in the upper rear section. Fig. 1 presents the tested RDC.

2.1.2. Thermosiphon thermal accumulator

The thermosiphon thermal accumulator is a rectangular container (92 × 11 × 26 cm) with a finned-tube heat exchanger. It was connected to the display cabinet evaporator via a riser and a downcomer (OD 12.7 mm, ID 10.9 mm) measuring 152 cm and 125 cm in height, respectively. Fig. 2 shows the internal structure and geometric details of the accumulator.

The container is filled with PCM, well-insulated with foam rubber, and strategically installed outside the refrigerated cell for optimal performance. The copper tubes and aluminium fins significantly increase the surface area for efficient heat transfer between the phase change material and the refrigerant flowing through the tubes. Positioning the accumulator outside the refrigerated cabinet maximises storage space for refrigerated products and allows unrestricted use of PCM. Additionally, the TTA uses the cabinet's refrigerant, which enhances heat transfer and thermodynamic efficiency and eliminates the need for a secondary refrigerant loop. The innovative accumulator is directly integrated into the existing display cabinet cooling circuit, allowing the system to operate efficiently with and without the accumulator (Fig. 3). While PCMs are well known for stabilising cabinet temperatures during compressor cycling and defrosting, their integration within the thermosiphon loop means this benefit is primarily harnessed during power outages, including scheduled DSM events.

The charging and discharging processes are independent of the type of evaporator used in the refrigeration unit. During the charging phase (only valves 3 and 5 closed), the refrigerant enters the accumulator, transfers some of the cold energy to the PCM (i.e. absorbs heat from the PCM), causing it to partially evaporate and the PCM to cool and solidify. The refrigerant then passes through the evaporator, exchanges with the cabinet's air and exits as a vapour to complete the vapour compression cycle. During the discharging phase (Demand-side management), rather than using a pump or any other electrical device, the process relies on the thermosiphon effect to supply the cold energy stored in the accumulator to the evaporator. When the compressor stops, the thermostatic expansion valve (TXV) sensing bulb – located at the evaporator outlet – warms up due to the absence of cold refrigerant flow. This temperature rise causes the TXV to temporarily open for about 2 to 3 min, lowering the pressure at the evaporator inlet. As a result, refrigerant flows naturally from the warmer condenser, through the open TXV and valves 1 and 2, into the cooler evaporator. At the same time, valve 4 is closed to block the evaporator outlet, trapping the refrigerant and ensuring the thermosiphon loop remains adequately charged for operation during the compressor-off phase. After this short transition period, valve 1 is closed and valve 5 is opened, forming a closed natural circulation loop between the evaporator and the accumulator. The refrigerant in the evaporator absorbs heat from the warm air inside the display cabinet and evaporates. Driven by the pressure difference, the vaporised refrigerant flows into the accumulator, where it condenses by absorbing the cold energy (i.e. releasing heat) previously stored in the PCM. In liquid form, the refrigerant returns to the evaporator by gravity, repeating the cycle until the PCM has no longer enough cold energy (i.e. no longer able to absorb heat by melting). During the charging phase, refrigerant flow is driven by the compressor. In the discharging phase, however, the flow direction is primarily governed by the positioning of the refrigerant pipes at the accumulator and evaporator. For instance, during discharging, liquid refrigerant consistently exits the accumulator through the lower pipe. The efficiency of the charging and discharging cycles depends on factors like the height difference between the accumulator and evaporator, the amount of refrigerant in the loop, and the pipe size [17,19,20]. The vapour compression system setup shown in Fig. 3 allows for an alternative configuration that excludes the accumulator (representing a standard plug-in display cabinet without modifications). In this configuration, only valve 5 is closed.

2.1.3. Display cabinet and accumulator instrumentation

Fig. 4 illustrates the system instrumentation. More than 30 calibrated T-type thermocouples (± 0.1 °C uncertainty) were installed in both the display cabinet and the TTA. Air temperature was monitored by 14 sensors, while 8 sensors tracked product temperature. 5 thermocouples measured the PCM temperature, and 2 others recorded the refrigerant temperature at the accumulator's inlet and outlet. Additional sensors were placed at the compressor's inlet and outlet, and at the condenser's outlet. Calibrated pressure sensors were also positioned at the compressor's inlet and outlet. Power consumption for the compressor, fan, electronics and lighting was measured with a wattmeter, and ambient temperature was continuously monitored. Data collection was managed with an Agilent 34970A system. Table 1 lists the main sensors along with their specifications and measurement uncertainties [17]. Air humidity is an important factor influencing cabinet thermal loads. Higher humidity means more moisture in the air, which requires additional energy to remove during cooling. This increases the cooling demand and raises the risk of condensation and frost, particularly on cold surfaces. Frost build-up can obstruct airflow and reduce cooling efficiency. No direct measurement of the controlled room's humidity was performed during the experiments. However, relative humidity was recorded afterward using a Mini Data Logger for temperature and humidity (model 174H BT). Absolute humidity was then estimated using an online calculator [21]. Within a day, the average absolute humidity in the experimental room, maintained at 16.22 ± 0.62 °C, was found to be 10.14 ± 0.92 g/m^3.

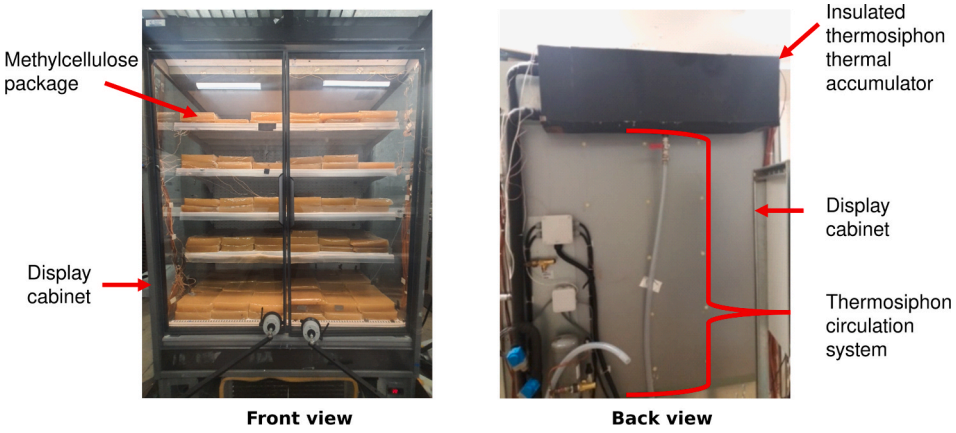

Fig. 1. Vertical closed-door refrigerated display cabinet with thermosiphon thermal accumulator.

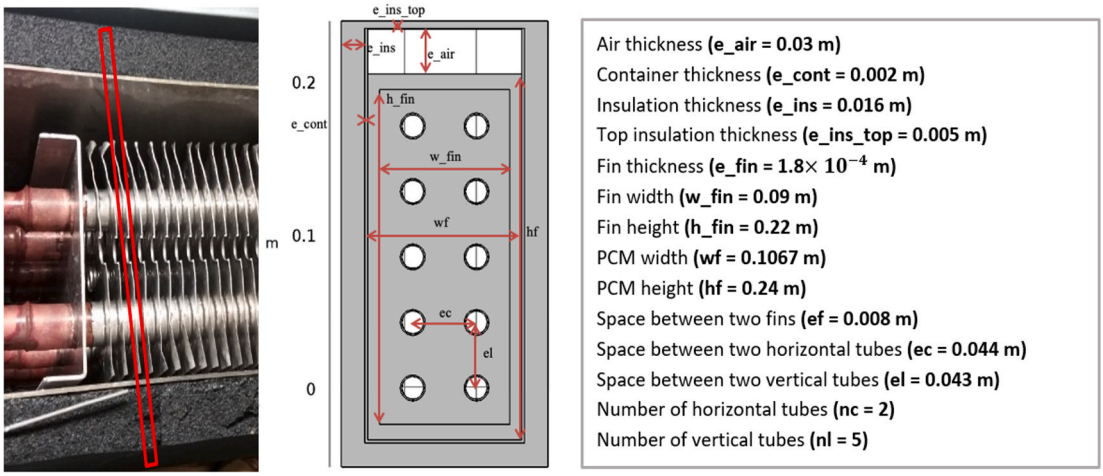

Fig. 2. Internal structure of the Thermosiphon Thermal Accumulator.

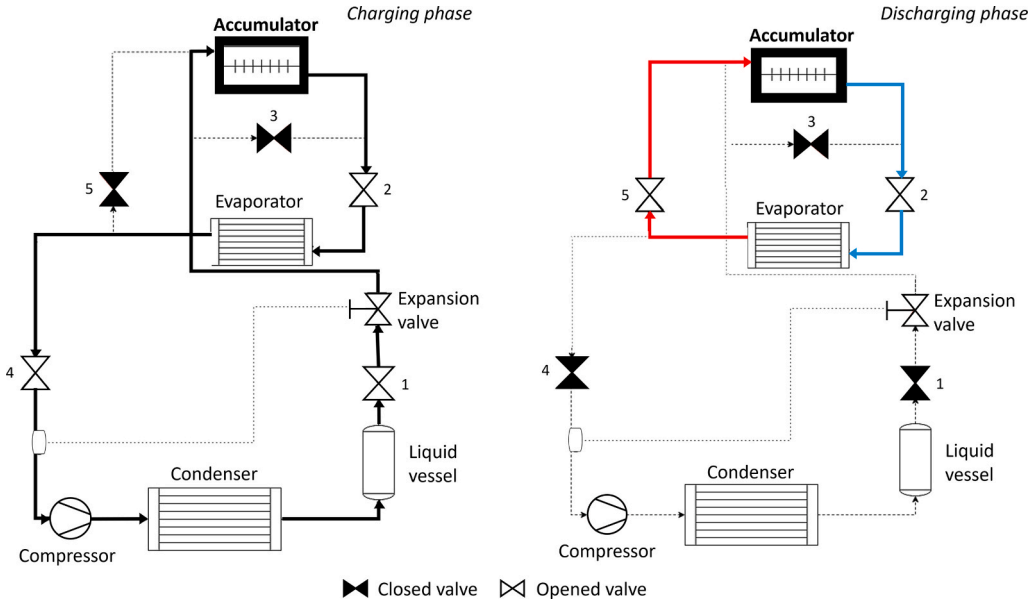

Fig. 3. Charging and discharging processes of the thermosiphon thermal accumulator integrated into the display cabinet's VCS.

2.2. Methods

This article evaluates the performance of a refrigerated display cabinet fitted with a thermosiphon thermal accumulator for demand-side management. The analysis focuses on five Key Performance Indicators (KPIs). Two experimental approaches were employed. The first set of experiments examined the accumulator's performance during a single DSM event across various operating conditions, aiming to assess how the novel system responds to changes in operating parameters and evaluate the reliability and efficiency of the TTA in consistently delivering cold energy without electricity. The second set of experiments investigated the accumulator's behaviour when DSM events were triggered at different times relative to defrost cycles and assessed the impact of running multiple DSM events within a single day.

2.2.1. Key Performance Indicators

- KPI 1: Activation of the thermosiphon loop

This first KPI is not a numerical value but assesses how effectively the system responds to DSM events. The thermosiphon (natural circulation loop) is considered successfully activated whenever the TTA transfers cold energy to the cabinet. This is observed through a decrease in air temperature inside the cabinet during DSM. Ultimately, this KPI indicates whether the thermosiphon successfully engages when requested.

- KPI 2: Time required to discharge the TTA during a DSM event ($\Delta t_{discharge}$&$t_{norm\,discharge}$)

The second KPI indicates how quickly the TTA discharges. The objective was to determine the time required for the accumulator to fully discharge (0 %) under different operating conditions. However, in some experiments, the PCM Solid Portion (SP_{av}) did not reach 0 % by the end of the DSM event. Therefore, to enable comparisons between scenarios, a discharge threshold from 50 % SP_{av} to 5 % SP_{av} was chosen to determine $\Delta t_{discharge}$ (Eq. (1)). By selecting these limits, the $\Delta t_{discharge}$ calculation excludes the initial rapid discharge (>50 %) and the final slow discharge (<5 %) of the TTA, focusing on a more stable and operationally relevant part of the discharge process, while also ensuring consistent comparability across test scenarios and reducing the influence of atypical or incomplete discharge behaviour. To further facilitate comparisons, a normalised (standardised) discharge time per percentage

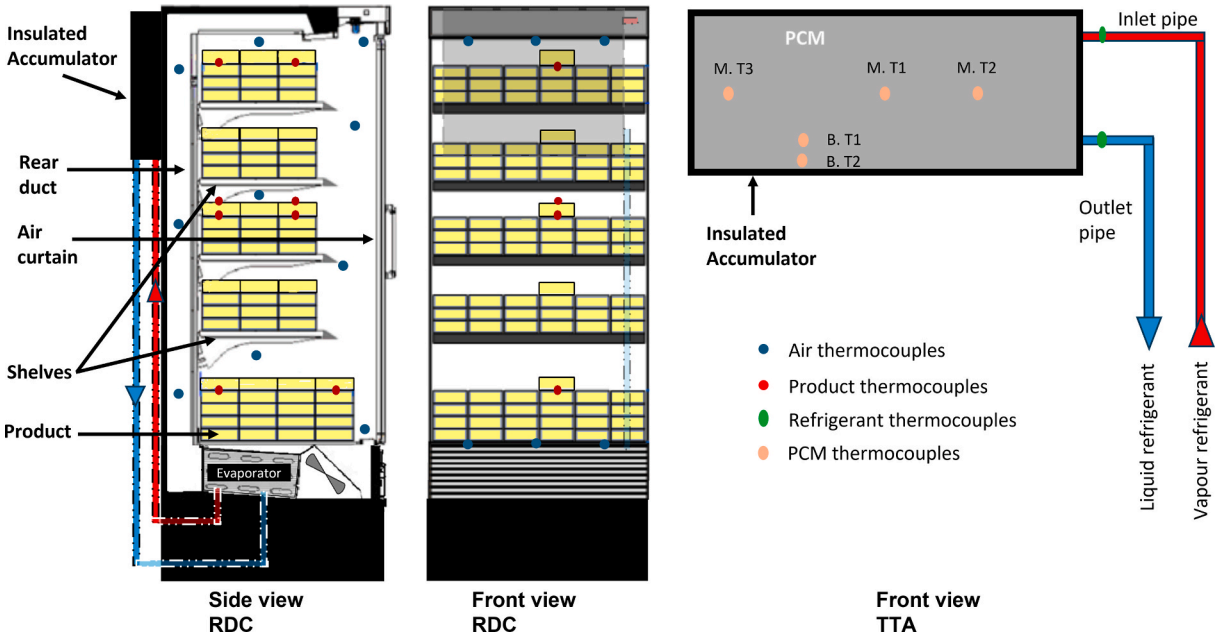

Fig. 4. Thermocouple arrangement for temperature measurements of air, product, PCM and refrigerant.

Table 1
Sensors and uncertainties (Yedmel et al. [17]).

Key measurement	Device	Range	Uncertainty
Temperature	Thermocouple T-type	−200_350 °C	± 0.1 °C
Pressure	P499 Electronic Pressure	−1_8 bar	± 0.18 bar
	Transducer	0_30 bar	± 0.60 bar
Electrical power	DIGIWATT	60_75 W	± 2.97 W
		450_1010 W	± 40.38 W

of energy released ($t_{norm_{discharge}}$) was defined (Eq. (2)). This metric indicates the time required to discharge 1 % of PCM within the specified interval.

$$\Delta t_{discharge} = t_{50\%} - t_{5\%} \quad (1)$$

$$t_{norm\,discharge} = \frac{t_{50\,\%} - t_{5\,\%}}{50\,\% - 5\,\%} \quad (2)$$

- KPI 3: Time required to charge the TTA after a DSM event (Δt_{charge} & $t_{norm_{charge}}$)

The third KPI measures how quickly the system recovers after a DSM event and, consequently, the potential number of DSM events per day. Δt_{charge} is calculated from a PCM SP_{av} of 5 % to a PCM SP_{av} of 50 % to ensure consistent comparisons between experiments (Eq. (3)). In fact, in some experiments, particularly those conducted under harsher conditions, higher PCM Solid Portions may not be reached within the 12-hour observation period due to factors such as defrost cycles or other limiting conditions. Using 50 % as a benchmark enables reliable comparison of system performance across different scenarios. Additionally, it ensures methodological consistency with the second KPI and focuses the analysis on the period where heat transfer is most active. A normalised charging time per percentage of energy absorbed (i.e., stored) ($t_{norm_{charge}}$) was also defined, representing the time required to charge 1 % of PCM (Eq. (4)).

$$\Delta t_{charge} = t_{5\ \%} - t_{50\ \%} \quad (3)$$

$$t_{norm_{charge}} = \frac{t_{5\ \%} - t_{50\ \%}}{5\ \% - 50\ \%} \quad (4)$$

The accumulator's Solid Portion defined for KPI 2 and KPI 3 was calculated based on the PCM's specific enthalpy distribution (Δh, in kJ/kg) provided by the supplier (Fig. 5). This distribution describes the thermal energy (kJ) associated with the phase change process per unit mass (kg) of PCM as a function of temperature. To express the degree of phase change, the specific enthalpy at a given temperature is normalised by dividing it by the latent heat of fusion L (kJ/kg) of the PCM. For each scenario, local PCM Solid Portion percentages are determined using five thermocouples positioned within the accumulator (Fig. 4), each measuring the temperature of a specific segment [17]. The Local PCM SP calculation is given by Eq. (5). The average PCM SP percentage (SP_{av}) is then calculated as the arithmetic mean of the SP percentages from all segments, each representing 20 % of the total value (Eq. (6)). SP_{av} provides a global estimation of the PCM's state of charge by considering multiple measurement points.

$$SP(\%) = \frac{\sum_{\Theta}^{\Theta_{max}} \Delta h(\Theta)}{L} \times 100 \quad (5)$$

$$SP_{av} = \frac{1}{5}\sum_{i=1}^{5} SP_i \quad (6)$$

- KPI 4: Product temperature rise during DSM

The fourth KPI measures how well the TTA can attenuate the impact of DSM on both core and surface product temperatures, and consequently, on product quality. The temperature rise was calculated by subtracting the product temperature at the start of a DSM event from the temperature at the end for different product positions in the display cabinet: top, middle, bottom, front, and rear (Fig. 4). The average rise in product temperature during the DSM event is then calculated for both core and surface temperatures within the cabinet.

- KPI 5: Energy consumption

The fifth KPI assesses the system's daily energy usage with and without a DSM event to identify potential overconsumption. Energy consumption was determined by averaging power consumption over a 12-hour period and extrapolating it to 24 h.

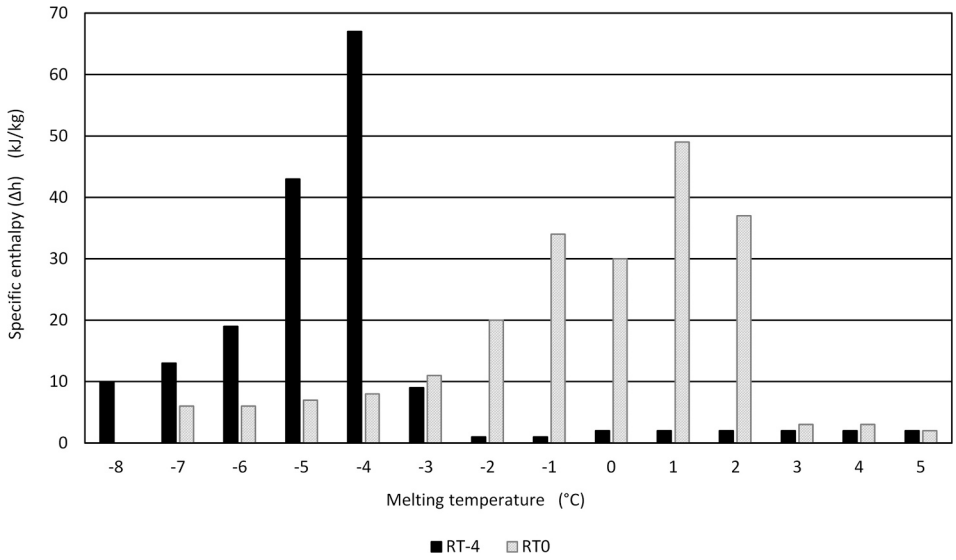

Fig. 5. Specific enthalpy distribution of RT-4 and RT0 (adapted from Rubitherm data sheets).

2.2.2. Impact of a single DSM event on thermosiphon thermal accumulator performance

Testing refrigeration systems under various operating conditions ensures product preservation standards and optimises energy efficiency, especially for novel or developing technologies. Previous research, such as Alzuwaid et al. [22], has highlighted that operating conditions significantly influence the energy-saving potential of phase change materials in display cabinets. Therefore, in this paper, the authors have evaluated the performance of the TTA across diverse operating scenarios to ensure its reliability and robustness. For each condition, two tests were conducted: one under regular operation and the other with a DSM event involving the discharge of the thermosiphon accumulator. The Key Performance Indicators analysis was crucial to validate the system's suitability for DSM and identify areas for improvement.

During a "DSM experiment", the compressor was intentionally shut down for 1.5 h while the system switched to discharging mode via control valves. This shutdown occurred only if the accumulator SP_{av} exceeded 75 % and the DSM event was well positioned between two defrost cycles. During this period, the evaporator fan remained active to facilitate heat transfer between the refrigerant and the air inside the cabinet, using just 7 % of the power required during regular operation. "Regular operation" refers to the normal functioning of the refrigerated display cabinet without any DSM strategy or accumulator discharge. Each experiment began at steady state. The testing protocol was rigorously conducted over 24 h for each set of conditions, alternating between two 12-hour cycles: one with a 1.5-hour DSM event and one with regular operation. This sequence was performed twice for each set of conditions to ensure reliable results. A total of 40 experiments were conducted, with various operating parameters, including ambient and thermostat temperatures, the percentage of the cabinet's storage volume occupied, the type of PCM used, and whether a door-opening regime was applied.

- Ambient and thermostat temperatures

Table 2 outlines the range of ambient and thermostat temperatures examined in the study.

Table 2
Tested Ambient and thermostat temperature values.

Parameter	Temperature value (°C)		
Ambient temperature	17	19	21
Thermostat set-up	−5	−3	−1

- Percentage of occupied storage volume

To accurately simulate supermarket conditions, three storage volume percentages were tested, covering scenarios from a fully loaded to a nearly empty cabinet (Fig. 6).

- Door opening regime

Tests were conducted with and without door openings. A programmable system with precise control over door openings was used to test two distinct operational regimes (Fig. 7). The first regime featured 6 door openings per hour, each lasting 12 s. This scenario reflects the average door usage observed by FRICKE and BECKER [23] and adheres to ANSI/ASHRAE [24] guidelines. The second regime followed the ISO [25] standards, simulating restocking activities. In this setup, each door was opened for 3 min to simulate replenishment, followed by 10 shorter openings per hour, each lasting 15 s. Note that Fig. 7 illustrates only the shorter openings and does not include the replenishment phase of the ISO [25] protocol.

- Phase change material type

This study investigated two types of phase change materials (PCMs), as detailed in Table 3. For each experiment, approximately 16.5 kg of PCM was used. Phase change temperature and heat storage capacity are key factors in selecting a PCM for demand-side management.

- Summary

Table 4 provides a detailed summary of the experiments conducted to evaluate the performance of the thermosiphon thermal accumulator.

2.2.3. Impact of multiple demand-side management events on thermosiphon thermal accumulator performance

In this paper, the authors have also examined how the timing of demand-side management (DSM) relative to defrost cycles affects the TTA efficiency and investigated the effects of implementing multiple DSM cycles within a single day on system performance.

- Demand-side management scheduling

Fig. 6. Tested occupied cabinet storage volume.

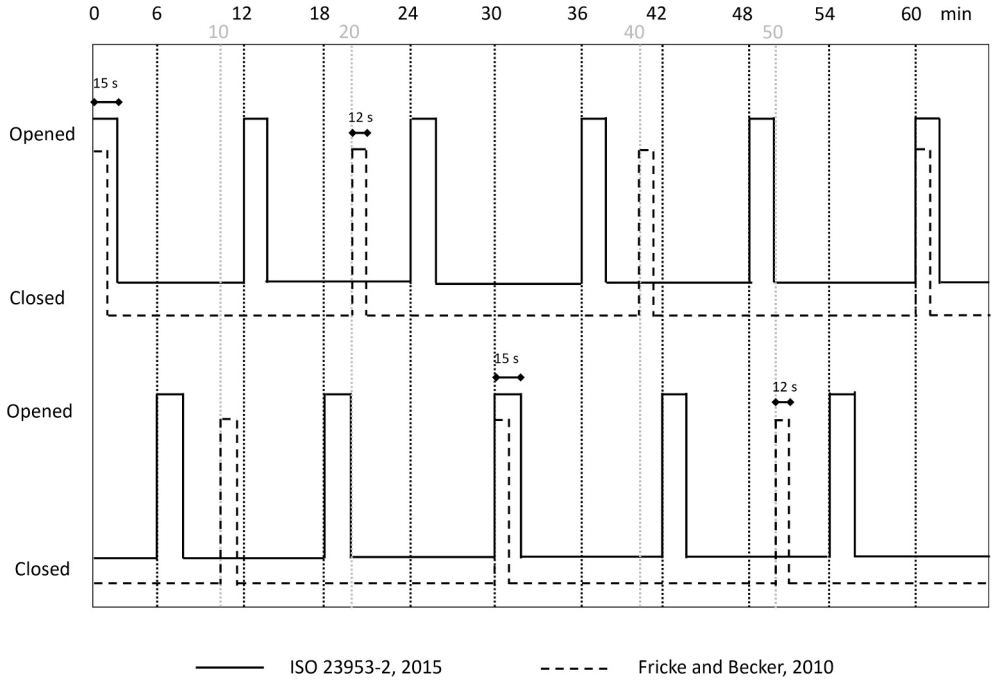

Fig. 7. Tested door opening regimes.

Table 3
Tested PCM characteristics.

PCM type	Phase change temperature (°C)	Liquid density at 15 °C (kg/l)	Heat storage capacity ± 7.5 % (kJ/kg)	Specific heat capacity (kJ/(kg.K))	Heat conductivity (W/(m.K))
RT0	−1 to 0	0.77	175	2	0.2
RT-4	−4 to −7	0.76	180	2	0.2

Research has consistently demonstrated that incorporating phase change material into refrigeration systems improves shelf and product temperature stability while reducing overall energy consumption, particularly during defrost cycles. Gin et al. [26] revealed that placing PCM panels along the internal walls of a freezer significantly slowed the temperature rise rate during a 30-minute defrost cycle, with a slight reduction in energy consumption compared to a freezer without PCM. In their review of latent heat and cold storage in domestic refrigeration, Mastani Joybari et al. [27] highlighted that PCM effectively reduces temperature fluctuations in air and products during defrost cycles. However, they noted that the compressor requires extended ON time to fully recharge the PCM once power is restored. Wu et al. [28] showed that their novel shelf, made of heat pipes and three types of phase change materials (RT3, RT4, and RT5), effectively reduced the core temperature of food packages during ON/OFF compressor cycles and minimised temperature fluctuations during defrosting periods in an

Table 4
Summary of all tested operating conditions.

Label	Ambient Temperature (°C)	Storage volume (%)	Thermostat Temperature (°C)	Door Openings	PCM Type	Test Type	Number of tests
E.01	19	50	−3	No	RT-4	Regular	2
E.02	19	50	−3	No	RT-4	1.5 h DSM	2
E.03	21	50	−3	No	RT-4	Regular	2
E.04	21	50	−3	No	RT-4	1.5 h DSM	2
E.05	19	90	−3	No	RT-4	Regular	2
E.06	19	90	−3	No	RT-4	1.5 h DSM	2
E.07	19	90	−1	No	RT-4	Regular	2
E.08	19	90	−1	No	RT-4	1.5 h DSM	2
E.09	19	90	−1	YES (ISO 23953–2)	RT-4	Regular	2
E.10	19	90	−1	YES (ISO 23953–2)	RT-4	1.5 h DSM	2
E.11	19	90	−1	YES (Fricke & Becker)	RT-4	Regular	2
E.12	19	90	−1	YES (Fricke & Becker)	RT-4	1.5 h DSM	2
E.13	19	10	−3	No	RT-4	Regular	2
E.14	19	10	−3	No	RT-4	1.5 h DSM	2
E.15	17	50	−3	No	RT-4	Regular	2
E.16	17	50	−3	No	RT-4	1.5 h DSM	2
E.17	19	90	−5	No	RT-4	Regular	2
E.18	19	90	−5	No	RT-4	1.5 h DSM	2
E.19	19	90	−1	No	RT0	Regular	2
E.20	19	90	−1	No	RT0	1.5 h DSM	2

open display cabinet.

All these findings are heavily influenced by the charging state of the PCM. In a pressured electrical grid scenario, power outages can be either voluntary or unplanned, and a well-designed DSM system must effectively manage these outages at any moment. Consequently, it is essential to determine whether the timing of demand-side management relative to defrost cycles impacts the accumulator performance. In the present paper, three different experiments were conducted to investigate it: one with a 1.5-hour DSM event with accumulator discharge implemented right before a defrost period, another immediately after, and a third positioned between two defrost periods. In all three experiments, the ambient temperature, thermostat setting, and occupied storage volume were maintained at 17 °C, −3 °C, and 90 %, respectively, with RT-4 used as the PCM. Each experiment lasted 24 h and was performed twice, with the results averaged across the two runs.

- Multiple demand-side management cycles

Testing multiple DSM events per day ensures that the thermosiphon thermal accumulator is reliable, responsive, and effective. A scenario with three DSM events, each lasting 1.5-hour, was compared to scenarios with two DSM events and a single DSM event. In all cases, the occupied storage volume was maintained at 50 %, the thermostat was set to −1 °C, and the ambient temperature was held at 19 °C, using RT-4 as the phase change material. Each experiment lasted 24 h and was repeated.

3. Results

3.1. Key Performance Indicator 1: Activation of the thermosiphon loop

In all experiments conducted to investigate the impact of varying operating conditions on TTA performance, the thermosiphon loop was successfully activated regardless of the conditions. This highlights the excellent design and proper placement of the accumulator for any situation, ensuring the system's reliability in triggering the discharge of the accumulator when there is no electricity.

The thermosiphon thermal accumulator reliability also extends to DSM scheduling with regard to defrost cycles. The results suggest that the timing of DSM events – whether right before, immediately after, or

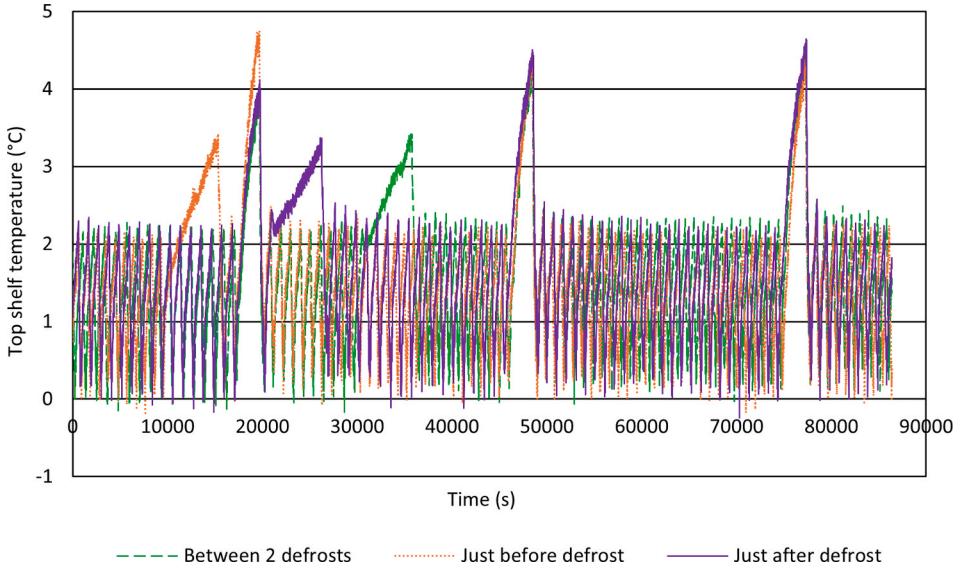

Fig. 8. Impact of DSM scheduling on top shelf temperature.

between defrost periods – has no significant effect on system activation, as the thermosiphon loop activates seamlessly in all cases, ensuring consistent temperature reduction. Fig. 8 depicts the variation in top shelf temperature across the three scenarios. The average shelf temperatures were measured at 0.60 °C, 0.72 °C, and 0.56 °C for the scenarios "Just before defrost", "Just after defrost", and "Between 2 defrosts", respectively, with a standard deviation of 0.08 °C. These averages were calculated by first determining the 24-hour mean temperature for each shelf level (top, middle, bottom), then averaging across all shelf levels, and finally taking the mean of the two repetitions. Daily energy consumption was recorded as 6.99 kWh for "Just before defrost", 6.73 kWh for "Just after defrost" and 6.86 kWh for "Between 2 defrosts", with a standard deviation of 0.13 kWh. Considering the standard deviations, the observed differences are not significant. However, it is worth examining the compressor's behaviour, as noted by Rocha et al. [9], to better understand the slight differences observed. One notable difference lies in the length of the defrosting period following each DSM event. Fig. 9 shows the compressor's operation, focusing on the length of the defrost cycle following each DSM event.

The average defrost time during regular operation is approximately 42 min. Following DSM, this duration increased by 3 % in the "Just before defrost" case and by 14 % in the "Just after defrost" case. In contrast, the "Between 2 defrosts" case showed a 4 % reduction in defrost time. Another key difference lies in the compressor operating time ratio. Under regular conditions, the compressor runs about 25 % of the time, but this changes in response to thermal loads on the cabinet. In the first ON/OFF cycle following the defrost period after the DSM event, the compressor operating time ratio rose to 52 % in the "Just before defrost" case and to 44 % in both the "Just after defrost" and "Between 2 defrosts" cases. The "Just before defrost" case experienced the largest increase in compressor runtime, with an additional 8 min, which could likely explain the slightly higher energy consumption observed in this scenario. The "Just after defrost" case returned to regular operation the fastest, with the compressor running at 26 % by the third ON/OFF cycle, compared to 32 % and 28 % for the "Just before defrost" and "Between 2 defrosts" cases, respectively. This quicker stabilisation could likely explain its slightly lower energy consumption. The compressor's behaviour helps explain the slight differences observed across the three scenarios.

In conclusion, although slight variations in energy consumption and average shelf temperature are observed when scheduling a DSM event before, immediately after, or between two defrost cycles, the timing of DSM has no impact on system activation, thereby validating the first KPI.

3.2. Key Performance Indicator 2 and 3: Time required to discharge and charge the thermosiphon thermal accumulator

Additional Key Performance Indicators included the time required for charging and discharging the Thermosiphon Thermal Accumulator. Fig. 10 illustrates $\Delta t_{discharge}$ and Δt_{charge} as a function of DSM experiments, ranging from E.02 to E.16.

As shown in Fig. 10, the time required to charge or discharge the PCM varies depending on operating conditions, with greater fluctuations observed during the charging phase. Experiments E.02, E.04, E.06, E.14, and E.16 exhibited similar trends, as $\Delta t_{discharge}$ was consistently longer than Δt_{charge}. More specifically, $\Delta t_{discharge}$ remained at approximately 1 h in all cases, whereas Δt_{charge} was less than 30 min for E.02, E.04, and E.06 and under 45 min for E.14 and E.16. This behaviour aligns with the findings of Rivera and Moraga [7], who observed that discharging time was consistently longer than charging time across all their numerical simulations on the performance of PCM plates attached to freezer walls.

However, this trend is not universal. Thermal load, compressor power and accumulator design are key factors that determine PCM charging (freezing) and discharging (melting) times, which are also influenced by the temperature difference between the inlet fluid at the accumulator entry and the PCM's eutectic point [29]. Consequently, experiments E.08, E.10, and E.12, which represent high thermal load scenarios, exhibited the opposite trend to experiments E.02, E.04, E.06, E.14, and E.16. In these cases, the charging period significantly exceeded the discharging period, with Δt_{charge} surpassing 2 h in all three experiments. Precisely, Δt_{charge} was recorded as 2.59 h for E.08, 2.14 h for E.10, and 3.15 h for E.12, whereas $\Delta t_{discharge}$ was around 40 min for E.10 and E.12, both of which involved door openings. In fact, during the charging period, the display cabinet's VCS must charge the PCM while maintaining a low internal temperature. As a result, charging takes longer when warm air infiltrates the cabinet. Experiments involving door openings required extended charging times due to the increased thermal load. Conversely, the discharging process was significantly faster, as air infiltration raised the cabinet temperature, prompting the PCM to release stored cold energy more rapidly through thermosiphon cooling.

In addition to air infiltration, the high thermostat setpoint in these three experiments further contributed to prolonged charging times, as less cold energy was transported by the refrigerant.

Fig. 10 also highlights the influence of the cabinet's occupied storage

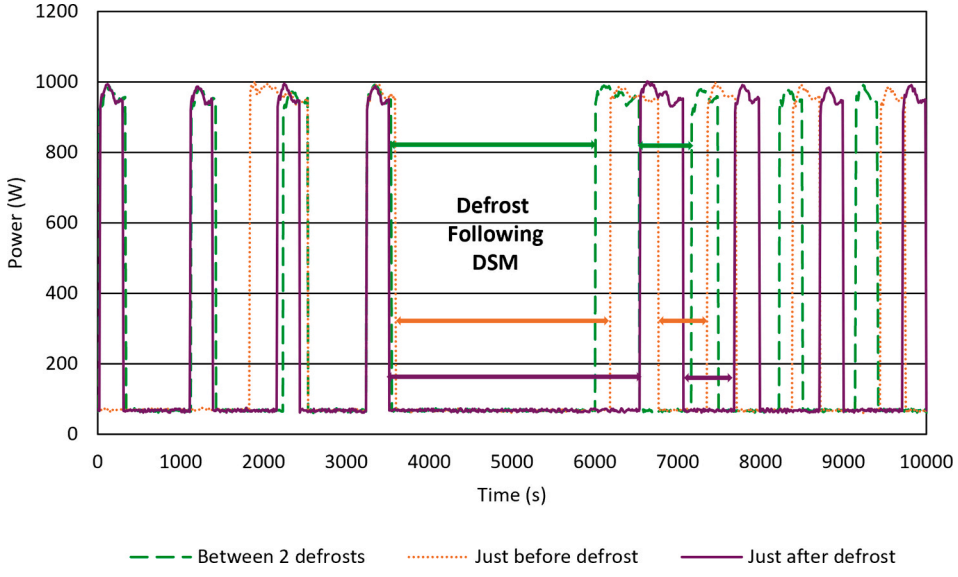

Fig. 9. Impact of DSM scheduling on compressor behaviour: focus on Post-DSM Defrost Cycle.

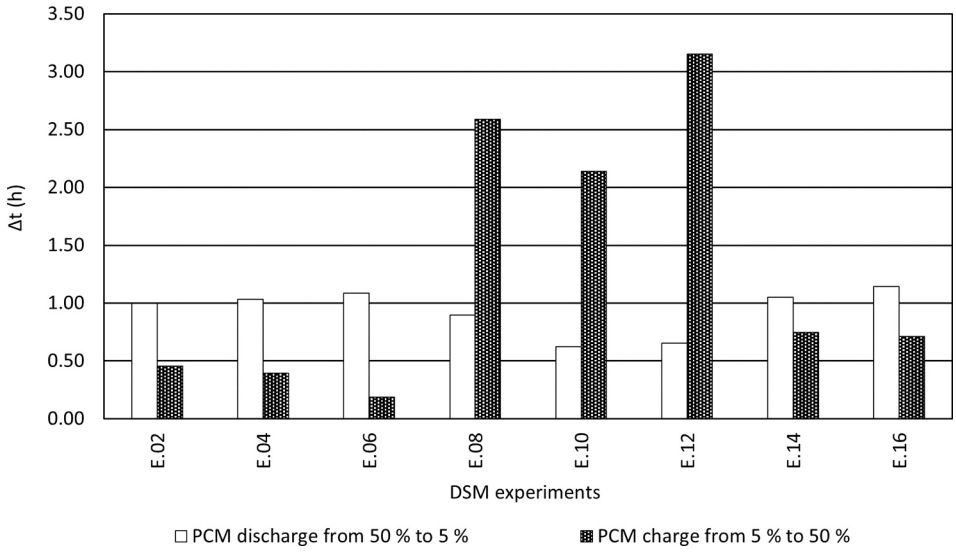

Fig. 10. Time required to partially charge and discharge the PCM.

volume on Δt_{charge}. Indeed, in experiment E.14, which represents an almost empty cabinet, the PCM took significantly longer to charge compared to experiment E.06, where the cabinet was fully loaded. To illustrate, Δt_{charge} was 45 min for E.14 but only 11 min for E.06. This suggests that a fully loaded cabinet reduces charging time, as stored products acquire thermal inertia, lowering the overall thermal load (PCM + cabinet air temperature) at the end of a DSM event. Raising cabinet load from 10 % to 50 % cut $t_{norm_{charge}}$, by 23 s/% of PCM and $t_{norm_{discharge}}$ by only 4 s/% of PCM. Beyond cabinet load, ambient temperature also influences these times. Increasing ambient temperature by 2 °C from 19 °C to 21 °C had little effect, but raising it from 17 °C to 19 °C cut $t_{norm_{discharge}}$ by 12 s/% and $t_{norm_{charge}}$ by 21 s/%. This shows charging is more sensitive to ambient temperature, though Ben-Abdallah et al. [6] found the opposite when PCM was placed in the rear duct, highlighting the impact of PCM positioning and cabinet design.

Experiments E.18 and E.20 are not included in Fig. 10 due to their atypical $\Delta t_{discharge}$ and Δt_{charge}. In these cases, the PCM SP_{av} reached only 10 % (E.18) and 45 % (E.20) by the end of the DSM event. In the case of E.18, the low SP_{av} resulted from the combined effects of a very low thermostat setpoint (−5 °C), optimal occupied storage volume, and ambient room conditions. Conversely, in E.20, despite the high thermostat setpoint (−1 °C), the TTA remained mostly charged, since RT0 has a higher phase change temperature range than RT-4 (Table 3). For these two experiments, $\Delta t_{discharge}$ and Δt_{charge} were determined based on a PCM SP_{av} range of 95 % to 50 %. It was observed that $\Delta t_{discharge}$ lasted around 30 min for E.18 and 1.09 h for E.20, both of which were shorter than Δt_{charge} (0.9 h for E.18 and 2.87 h for E.20).

When considering the charging process from a PCM SP_{av} of 50 % to 95 %, lowering the thermostat set temperature by 2 °C [from −3 °C (E.06) to −5 °C (E.18)] significantly reduced Δt_{charge} from 2.11 h to 0.9 h. This reduction occurs because a lower thermostat setting increases compressor operation, enhancing refrigerant cooling efficiency and accelerating PCM charging. This result aligns with Ben-Abdallah et al. [6], who reported a 2-hour reduction in charging time when decreasing the thermostat set-up temperature. In experiment E.06, charging from a PCM SP_{av} of 5 % to 50 % took only 11 min, whereas charging from 50 % to 95 % required 2.11 h. This significant difference can be explained by the varying thermal resistance during phase change. At the beginning of PCM charging process, the temperature difference between the liquid PCM and the refrigerant is greater, allowing rapid freezing. However, when the solidification starts at the heat exchanger surface, a PCM solid layer forms while much of the material remains liquid. As more of the PCM solidifies, the remaining liquid becomes trapped within a growing solid structure, which acts as an insulator. The insulating effect of the frozen PCM significantly slows down charging above 50 %. Additionally, periodic defrost cycles occurring every 8 h further extend the charging time. As expected, experiments under the highest heat loads – caused by high thermostat settings or frequent door openings – exhibited the longest charging and the shortest discharging times. However, when the thermal load was primarily due to elevated ambient temperatures, Fig. 10 reveals an opposite trend: charging times decreased as ambient temperature increased. This counterintuitive behaviour is attributed to increased compressor runtime under high ambient conditions, which enhances the system's cooling capacity during the charging phase. This effect is reflected in the display cabinet's higher energy consumption.

Experiments E.10 and E.12, simulating door openings, are more representative of supermarket conditions, whereas the other scenarios correspond to private use. In E.10, under the ISO door-opening scenario, the accumulator reached 77 % SP_{av} about 6 h after DSM, theoretically allowing up to three DSM events per day with the current TTA design. The system's reliability under multiple DSM events was investigated by comparing scenarios with one, two, and three compressor shutdowns at 19 °C, 50 % occupied storage volume, −1 °C, and RT-4 as PCM. Fig. 11 presents the variation in bottom shelf temperature with TTA SP_{av} across the three scenarios. The average shelf temperatures for the scenarios with 1 DSM, 2 DSM, and 3 DSM were 2.24 °C ± 0.07 °C, 2.40 °C ± 0.16 °C, and 2.61 °C ± 0.06 °C, respectively. These results indicate that increasing thermal loads by implementing multiple DSM events throughout the day only slightly raises cabinet temperatures, which remain below the levels observed during defrost periods. This performance can be attributed to the activation of the thermosiphon loop on demand (KPI 1). Regarding temperature increase, each DSM event in the three scenarios did not result in the same rise in air temperature: the second DSM event in Fig. 11b and Fig. 11c was associated with the most significant temperature increase. This variation can be explained by the accumulator SP_{av} at the start of each DSM event, which represents the amount of energy stored in the PCM.

A higher PCM Solid Portion corresponds to a greater amount of energy available that can be returned to the cabinet. Conversely, lower SP_{av} result in less power being delivered through the thermosiphon during DSM events, leading to higher temperatures at the end of the event. For instance, the second DSM event was triggered when the TTA SP_{av} reached 40 %, compared to 75 % at the start of the first DSM event. In the scenario with 1 DSM, the accumulator reached 50 % SP_{av} approximately 2 h and 40 min after a DSM event and 75 % SP_{av} (the

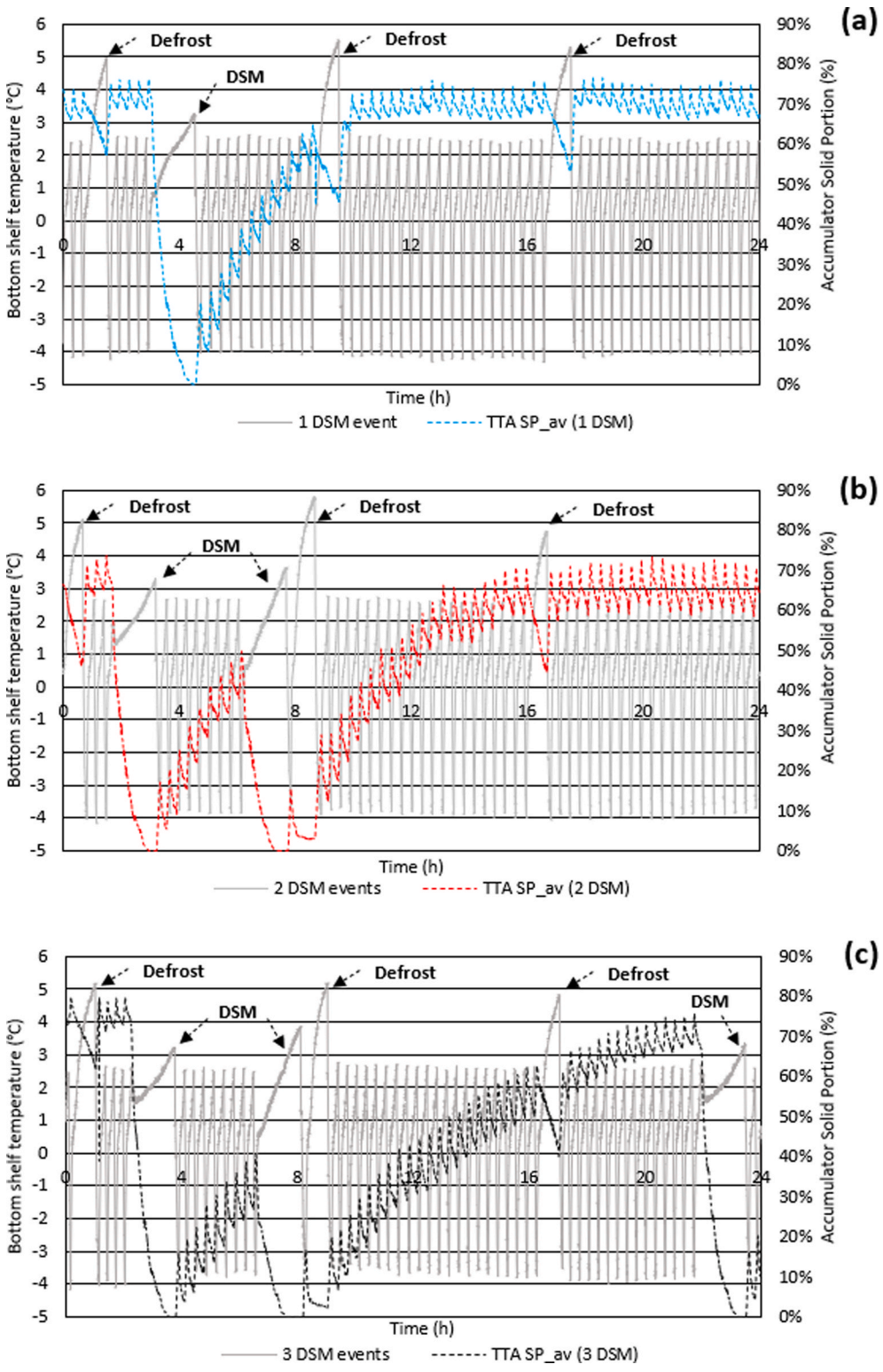

Fig. 11. Impact of multiple DSM events on bottom shelf temperature and accumulator SP_{av}: (a) 1 DSM scenario; (b) 2 DSM scenario; (c) 3 DSM scenario.

starting percentage) after 8 h. Under the same operating conditions, and if the TTA is consistently recharged to 75 % before each DSM event, the accumulator can effectively support two DSM events of 1.5 h each per day. Under E.06 operating conditions, starting with a SP_{av} of 90 %, the system can maintain low temperatures during five DSM events of 1.5-hour each, spaced 3 h apart.

In conclusion, the TTA can handle multiple DSM events without any decline in performance, provided there is sufficient time for recharging between events. Under the operating conditions tested in this study, the required full recharging time ranges from 2.5 to 8 h. Cabinet thermal loads and PCM phase change temperature significantly influence the charging and discharging processes of the TTA. These factors must, therefore, be carefully assessed when determining the appropriate amount of PCM and the cabinet operating conditions needed to achieve the desired number of daily DSM events. Key Performance Indicators 2 and 3 are verified.

3.3. Key Performance Indicator 4: Product temperature rise during demand-side management

PCMs are highly effective in limiting temperature increases during compressor-off periods; however, extreme external influences may exceed their ability to fully neutralise temperature rises [28]. The extent of product temperature rise inside a closed refrigerated display cabinet during heat loads, such as door openings or compressor shutdowns, depends on product placement within the cabinet [17,30]. In this paper, product temperature rise is not presented as a function of position. Instead, Fig. 12 presents the fourth KPI: the average increase in the core and surface temperatures of products during a DSM event in the closed refrigerated display cabinet.

The results indicate that high door-opening frequency and elevated ambient temperatures significantly increase product temperatures during DSM. Nevertheless, the core temperature rise remains below 0.5 °C across all operating conditions. The highest core temperature increase, 0.42 °C, occurs in E.10, which simulates the ISO door-opening scenario. Surface temperature rises were well below 1 °C, with the highest values observed in E.04 (0.79 °C) and E.10 (0.76 °C). A higher storage volume percentage also reduced the temperature rise due to the increased thermal inertia of the stored products.

According to EVAIN [31], a product is considered compliant if its core temperature rise remains below or equal to 1 °C and its surface temperature rise remains below or equal to 2 °C relative to the regulatory temperature. The Thermosiphon Thermal Accumulator proved effective in preserving product quality even during a 1.5-hour DSM event by maintaining cabinet temperatures lower than those observed in cabinets undergoing DSM without any PCMs. Yedmel et al. [17] reported that DSM without PCM results in significantly higher increases in both air and product temperatures. Their study observed a 270 % higher rise in product core temperature during DSM without PCM compared to systems using the TTA. Specifically, the average product core temperature rise with the TTA was 0.2 °C, while without the TTA, it was 0.7 °C. In this paper, the core temperature rise observed in experiment E.10 clearly indicates that without the TTA, the product core temperature would exceed the regulatory limit.

Fig. 12 also reveals that experiment E.20 exhibited the second-highest increase in product core temperature despite having the highest PCM SP_{av} at the end of DSM (41 %). This outcome is attributed to the thermophysical properties of the PCM used (RT0), particularly its phase change temperature and heat storage capacity (Table 3). Mastani Joybari et al. [27] mentioned that the PCM's ability to maintain low temperatures and buffer the effects of a power outage depends on its thermal load and the external thermal load, including ambient conditions and cabinet heat generation.

In summary, the fourth KPI is validated. It confirms that the Thermosiphon Thermal Accumulator effectively maintained product temperatures within regulatory limits under all tested operating conditions, ensuring product quality during a 1.5-hour DSM event. This performance results from the balance between energy storage capacity and heat transfer dynamics. While the PCM's heat storage capacity and quantity define the total energy stored in the accumulator, the temperature gradient between the PCM and its surroundings (cabinet and ambient conditions) dictates the heat transfer rate during power outages.

3.4. Key Performance Indicator 5: energy consumption

The final key performance indicator is the energy consumed by the system. Table 5 presents the values of the daily energy consumption of the cabinet during tests with a single DSM event and regular operation, both measured using a wattmeter. Fig. 13 provides a graphical comparison of these values.

According to Fig. 13, higher daily energy consumption (> 7 kWh)

Table 5
24-hour measured energy consumption for DSM and regular experiments.

Experiments	Energy consumed in 24 h (kWh)		
	Regular	DSM	Reduction
E.01/E.02	7.04	6.71	−4.6 %
E.03/E.04	8.47	8.33	−1.6 %
E.05/E.06	6.76	6.73	−0.5 %
E.07/E.08	6.52	6.08	−6.7 %
E.09/E.10	7.59	7.29	−3.8 %
E.11/E.12	7.30	6.76	−7.4 %
E.13/E.14	7.30	7.15	−2.1 %
E.15/E.16	6.31	6.10	−3.4 %
E.17/E.18	6.97	6.77	−2.7 %
E.19/E.20	6.83	6.52	−4.5 %

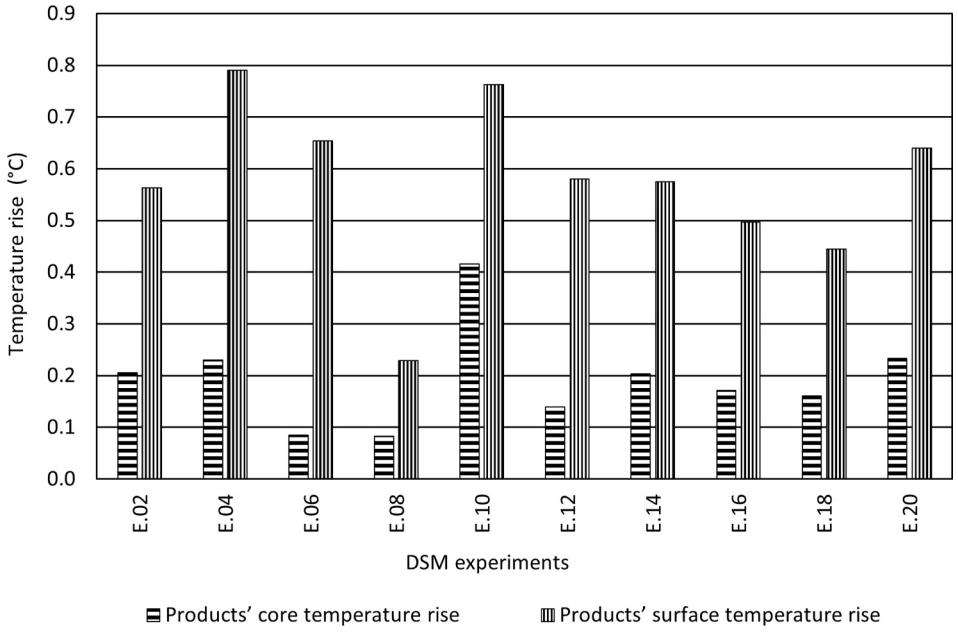

Fig. 12. Products' temperature rise during DSM.

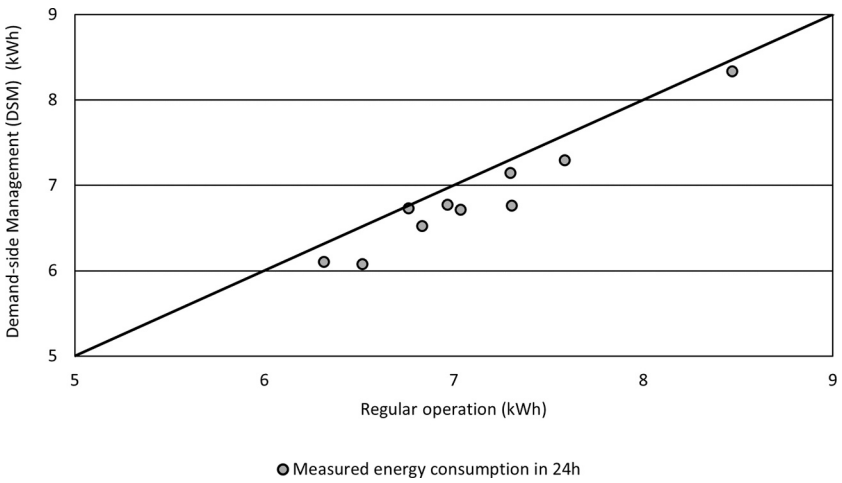

Fig. 13. 24-hour energy consumption comparison: DSM vs. regular operations.

was observed in experiments with significant heat loads, including high ambient temperatures, low storage volume, and door openings. This is attributed to the extended operation time of the compressor, which is required to remove the additional heat. The highest measured energy consumption was recorded in experiment E.03, with 4.23 kWh consumed over 12 h, resulting in a daily consumption of 8.47 kWh. Across all experiments, the system does not consume more energy during DSM than during regular operation. For instance, the energy use for E.04 was approximately 2 % lower than for E.03, with a daily energy consumption of 8.33 kWh. The most significant deviation between daily energy consumption during DSM and regular operation was a 7 % reduction, observed in experiments E.07/E.08 and E.11/E.12. Experiments E.05/E.06 showed the slightest deviation, with almost no difference between DSM and regular operation.

The reduction in energy consumption could be unexpected, as one might assume that the system would consume more energy during the TTA charging and discharging phases due to thermal losses and heat transfer inefficiencies. However, energy savings due to PCM or the combination of a thermosiphon and PCM is not uncommon and has already been observed in other studies. To the best of the authors' knowledge, no results have been found in the literature for a study coupling a thermosiphon with PCM for demand-side management purposes. For example, Gin et al. [26] added PCM panels along the internal walls of a freezer and compared energy consumption with and without PCM during defrost cycles and door openings. They observed a 7–8 % reduction in energy consumption during defrost cycles and door openings when using PCM panels, compared to experiments without. Since defrosts and door openings introduce thermal loads to the cabinet – similar to a DSM event – one could expect a similar outcome during DSM events. In addition, Azzouz et al. [32] found that placing PCM on the back of a refrigerator's evaporator improved the COP by 10–30 %, depending on the thermal load and PCM type. Notably, Foster et al. [33] compared the energy consumption of electric defrosting to that of a thermosiphon coupled with PCM for display cabinet defrosting. Their results showed that the thermosiphon defrosting consumed 3.65 kW less than the electric defrosting.

In this paper, a slight reduction in energy consumption was observed during DSM experiments (DSM events with TTA discharge) compared to regular operation (no DSM events and no TTA discharge). To better understand these findings, further analyses were conducted on the behaviour of the compressor, condenser, and evaporator during both DSM and regular operations.

3.4.1. *Compressor analysis*

It was observed that, for the same duration – containing one defrost cycle for regular operations and one DSM event along with one defrost cycle for DSM experiments – the average compressor operating time ratio was lower for the DSM experiments. For example, the average operating time ratio was 22 % ± 0 % for E.15, compared to 20 % ± 1 % for E.16 across both runs. This suggests that the compressor operates approximately 2 % less during DSM than regular operation, a trend observed in all experiments. For E.01 and E.02, the average compressor operating time ratios were 24 % ± 0 % and 22 % ± 1 %, respectively, while for E.03 and E.04, the ratios were 32 % ± 2 % and 29 % ± 2 %, respectively. In the set of experiments involving temperature changes (E.01/E.02, E.03/E.04, and E.15/E.16), energy consumption during regular operation was found to be about 1.03 ± 0.02 times higher than during DSM. The compressor operating time ratio during regular operation was about 1.11 ± 0.01 times higher during regular operation compared to DSM. Given the uncertainties, it can be concluded that the compressor operating time ratio likely accounts for the observed variation in energy consumption between DSM and regular operations.

Additionally, the number of compressor restarts was lower for all the tests in the DSM experiments. A compressor restart is defined as the start of an ON cycle. Even when the total number of complete ON/OFF cycles is the same for regular and DSM experiments, regular operation tends to involve one or two additional compressor restarts, especially under harsher operating conditions. This indicates that the compressor undergoes fewer restarts during DSM experiments than during regular operation. Furthermore, an analysis of the instantaneous power revealed that each compressor restart is accompanied by a significant power spike, sometimes exceeding 2000 W and lasting less than 1 s. Due to the data acquisition system's limitations, recording data at tiny time intervals was impossible. To address this, a video of the instantaneous power measured by the wattmeter was recorded, allowing the identification of these peak power values. Fig. 14 presents power measurements during one compressor ON/OFF cycle. Power values were recorded every second for a few seconds before and after the start-up (from 0 to 5 s and 6 to 9 s), along with three additional high-frequency samples within the critical one-second window of the start-up peak (at precisely 5.2 s, 5.35 s, and 5.6 s), allowing precise capture of the brief but significant power spike during compressor start-up. This increase is likely due to an imbalance in the compressor during the OFF period when refrigerant pressure and temperature are not yet in equilibrium. Since these power spikes are brief compared to the overall running time, they alone cannot account for the reduction in energy consumption observed. However, fewer compressor restarts may allow the system to operate more stably and efficiently. These observations regarding compressor behaviour may help explain the energy consumption differences between DSM and regular operations.

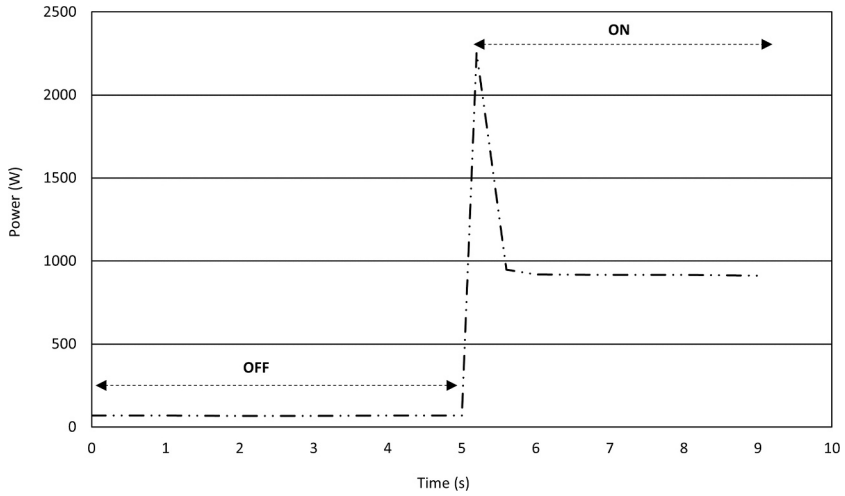

Fig. 14. Power peak observed during compressor start-up.

3.4.2. Charging period analysis

Another potential explanation of energy consumption reduction with DSM lies in the positioning of the Thermosiphon Thermal Accumulator. Integrated within the cabinet's refrigeration system, just before the evaporator, the TTA acts as an extension of the evaporator, increasing the heat exchange surface area. This expanded surface allows the refrigerant to vaporise at a more stable and higher pressure, enhancing the compressor's efficiency. This effect is particularly evident during the charging phase of the TTA (Fig. 15). The average evaporator pressure during the charging period in experiment E.04, calculated across the two runs, was 3.22 bar $\pm$ 0.03 bar. This represents a 5 % increase compared to experiment E.03, which showed an average of 3.07 bar $\pm$ 0.06 bar for the same period. As expected, this increase in evaporator pressure was accompanied by a slightly elevated evaporation temperature, particularly evident immediately after the DSM event.

However, an improvement in COP under these conditions is only valid if the condensing temperature remains constant or decreases. In the observed experiments, the increase in evaporator temperature during charging was accompanied by a simultaneous rise in condensing temperature. When this occurs, the thermodynamic efficiency of the cycle is reduced, as this pair negatively affects the COP. This indicates that the charging process alone cannot fully account for the energy savings observed. Rather, it is during the charging phase that the rebound effect becomes most evident. The rebound effect refers to the system's response to the thermal load accumulated during the DSM event [34]. To restore target conditions, the system operates at a higher capacity, resulting in temporarily elevated energy consumption and increased system effort. Nevertheless, when evaluating the entire test period, the data reveal a slight overall decrease in condensing temperature and increase in evaporator temperature, which together suggest a probable improvement in COP over the full duration of the experiment.

3.4.3. Analysis of the coefficient of performance (COP)

A quantitative analysis was carried out to deepen the thermodynamic interpretation of the energy savings by determining the coefficient of performance (COP) over the entire 12-hour period (Eq. (7)). Demand-side management experiments are expected to exhibit better thermodynamic performance – that is, a higher real COP – as they consumed less electrical energy. To estimate the Carnot COP, the average evaporator and condenser temperatures over the experiment were used (Eq. (8)). This provides the theoretical maximum COP for each operating condition.

$$\eta_{ex} = \frac{COP_{real}}{COP_{carnot}} \quad \Rightarrow \quad COP_{real} = \eta_{ex} \times COP_{carnot} \tag{7}$$

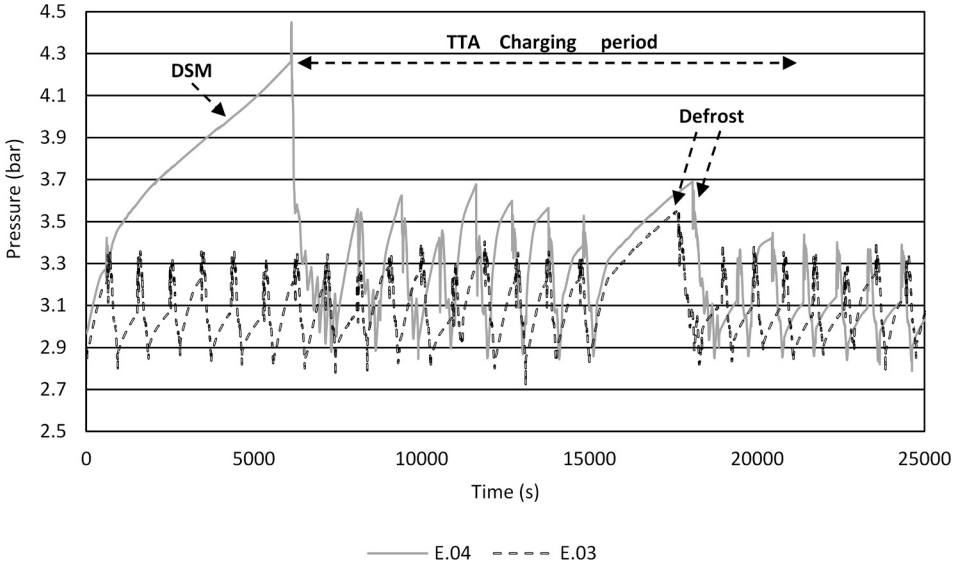

Fig. 15. Comparison of compressor inlet pressure trends in experiments E.03/E.04, focusing on the TTA charging phase.

$$COP_{real} = \eta_{ex} \times \frac{T_{evaporator_{av}}}{T_{condenser_{av}} - T_{evaporator_{av}}} \quad (8)$$

As detailed component-level data – particularly refrigerant mass flow rate – were not available, it was not possible to directly determine the cooling capacity or quantify entropy generation. Therefore, a thermodynamic benchmarking approach was adopted based on COP comparisons. It was assumed that both systems operate with similar exergy efficiency (Eq. (9)), a reasonable assumption when comparing similar types of refrigeration equipment operating under comparable conditions. Under this assumption, comparing Carnot COPs provides a valid thermodynamic basis for interpreting the observed reduction in energy consumption, despite the lack of detailed internal data. In essence, if a system has a higher Carnot COP and similar exergy efficiency, it should exhibit a higher real COP and therefore consume less electricity for the same cooling output.

Using the ratio of Carnot COPs, the real COP during DSM operation was estimated (Eq. (10)). The analysis showed that the real COP during DSM was approximately 1.02 times that of regular operation for experiments E.01 to E.06 and E.13 to E.16.

$$\eta_{ex_{DSM}} = \eta_{ex_{regular}} \quad \Leftrightarrow \quad \frac{COP_{real_{DSM}}}{COP_{carnot_{DSM}}} \approx \frac{COP_{real_{regular}}}{COP_{carnot_{regular}}} \quad (9)$$

$$COP_{real_{DSM}} = \frac{COP_{carnot_{DSM}}}{COP_{carnot_{regular}}} \times COP_{real_{regular}} \quad (10)$$

3.4.4. Synthesis

One observation emerging from the analysis is that, when estimating energy consumption from the end of the DSM event until the end of the test period, the energy consumption was higher in the DSM experiments compared to the same timeframe under regular operation. This outcome can be attributed to the well-known rebound effect. During the DSM event, compressor operation is reduced, leading to a temporary deviation from set operating conditions. Following the DSM event, the system must compensate for the accumulated thermal load by operating more intensively. This typically results in increased energy use.

However, despite this temporary rise in energy demand, it is possible that the rebound effect did not fully offset the energy savings achieved during the DSM event. Furthermore, the short-term increase in energy consumption may become diluted over a longer observation period, allowing the long-term energy savings from the DSM event to emerge more clearly. Therefore, while the rebound may dominate immediately after the DSM event, an extended evaluation period could reveal a net reduction in overall energy consumption and potentially improved system performance. This suggests that DSM interventions can, under appropriate conditions, yield meaningful long-term energy benefits, even when followed by a short-term recovery phase.

This confirms that the fifth KPI is met: the thermosiphon thermal accumulator effectively maintains product temperatures well below regulatory limits during a demand-side management event while not consuming more energy than during regular operation. The reduction in energy consumption observed during a single DSM event with accumulator discharge should be even more visible with multiple DSM events. Fig. 16 shows the cabinet's energy consumption during multiple DSM events with TTA discharge. The energy consumption for a single DSM event was 6.28 kWh ± 0.04 kWh, compared to 6.25 kWh ± 0.13 kWh for two DSM events and 5.98 kWh ± 0.02 kWh for three events. This confirms that an increase in DSM events with TTA discharge leads to a more significant reduction in energy consumption.

3.5. Cost-benefit analysis of thermosiphon thermal accumulator integration

A basic cost-benefit analysis was conducted to evaluate the installation of a thermosiphon thermal accumulator (TTA) on a closed refrigerated display cabinet, assuming one DSM event per day. The payback time was calculated using the ratio of initial costs to annual financial benefits (Eq. (11)).

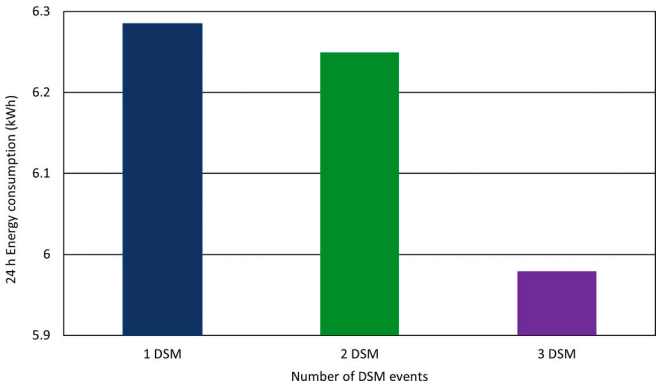

Fig. 16. Influence of multiple DSM events on daily energy consumption.

$$\text{Payback time} = \frac{\text{Initial costs}}{\text{Annual benefits}} \quad (11)$$

The initial cost was estimated at approximately 633 €, and included the following components: flow control devices for the thermosiphon loop (8 %), a liquid vessel to maintain refrigerant balance (3 %), 16.5 kg of phase change material (30 %), a finned-tube heat exchanger (47 %), and labour for installation (11 %).

Adopting demand-side management practices can generate revenue through electricity cost savings, direct financial compensation (in €/kWh shifted or avoided), preferential tariffs, and other incentives. In this analysis, only electricity cost savings and direct financial compensation were taken into account. Electricity cost savings were calculated using the European average business electricity rate of 0.186 €/kWh [35], ensuring consistency with the DSM direct financial compensation value of 0.95 €/kWh, which is based on Irish market data [36]. Using these compatible European-based values allows for a coherent and meaningful comparison in the financial analysis. The total annual benefit was estimated at 224 €, of which 16 % resulted from reduced electricity costs and 84 % from DSM-related income. The resulting payback period was approximately three years, which could be significantly shortened by performing multiple DSM events per day and accounting for all potential income streams from DSM practices. Conversely, it may increase slightly depending on regional energy prices and specific DSM market conditions.

4. Conclusion

This study investigates the ability of a novel thermosiphon thermal accumulator (TTA) to perform reliably and consistently under various operating conditions, along with its energy consumption and cost-benefit analysis, within the context of demand-side management (DSM). In contrast to a previous study – which introduced the TTA's working principle and assessed its temperature regulation under a single operating condition – the current work significantly broadens the scope by evaluating the TTA's performance across a range of ambient and thermostat temperatures, product loads, door-opening scenarios, and types of PCMs. Furthermore, unlike the earlier study, this research also examines the TTA's capability to handle multiple DSM events within a single day, providing a more realistic assessment of its operational potential. The results showed that:

- By combining the benefits of latent heat storage and the thermosiphon effect, the TTA consistently delivered cold energy to the cabinet

across all scenarios, maintaining product temperatures within regulatory limits.

- Charging and discharging performance was strongly influenced by operating conditions and thermal loads. Under high thermal loads, the accumulator discharged more rapidly and required over two hours to recharge. In contrast, lower thermal loads allowed for a 50 % recharge in just 30 min. Higher thermal loads also resulted in greater product temperature increases and higher energy consumption.
- Nonetheless, across all tested conditions, DSM operation did not lead to higher energy consumption compared to regular operation. In fact, energy use decreased by up to 7 % in some cases with the COP being approximately 2 % greater than under standard operating conditions. Although a rebound effect was observed, it did not completely negate the energy savings achieved during the DSM event, resulting in a net gain in energy efficiency.

The findings highlight the TTA's potential as a reliable and energy-efficient solution for DSM applications in both commercial and domestic refrigeration. Its ability to maintain temperature compliance without additional energy consumption positions it as a promising technology for integrating renewable energy sources, alleviating grid stress, and reducing CO_2 emissions. The economic analysis, taking into account electricity prices and investment costs, indicated that investment in the Thermosiphon Thermal Accumulator is economically viable, with a payback period of approximately three years based on European data. Future work will focus on optimising the TTA through a detailed analysis of the two-phase thermosiphon loop and accumulator design.

CRediT authorship contribution statement

Maria Aurely Yedmel: Writing – review & editing, Writing – original draft, Visualization, Validation, Methodology, Investigation, Formal analysis, Data curation. **Anthony Delahaye:** Writing – review & editing, Validation, Supervision, Formal analysis. **Denis Leducq:** Writing – review & editing, Validation, Supervision, Funding acquisition, Formal analysis, Conceptualization.

Funding

This work was part of the ENOUGH project supported by the European Union's Horizon 2020 research and innovation programme [grant number 101036588].

Declaration of competing interest

The authors declare that they have no known competing financial interests or personal relationships that could have appeared to influence the work reported in this paper.

Data availability

Data will be made available on request.

References

[1] IIR. (2022). Les grandes tendances du marché mondial du froid commercial. Retrieved from https://iifiir.org/fr/actualites/les-grandes-tendances-du-marche-mondial-du-froid-commercial#:~:text=Le%20march%C3%A9%20mondial%20du%20froid%20commercial%20a%20progress%C3%A9%20de%208,50%2C4%20%25%20en%202021.

[2] Business_Research_Insights. (2024). Refrigerated Display Cabinets Market Size, Share, Growth, and Industry Analysis, By Type (Frozen Type, Chilled Type), By Application (Beverages, Food, Medicine, Other), Regional Insights and Forecast to 2032. Retrieved from https://www.businessresearchinsights.com/market-reports/refrigerated-display-cabinets-market-110748.

[3] Unido. Towards energy efficient retail refrigeration in developing countries. 6th IIR International Conference on Sustainability and the Cold Chain. Retrieved from. 2020.

[4] Alzuwaid FA, Ge YT, Tassou SA, Raeisi A, Gowreesunker L. The novel use of phase change materials in a refrigerated display cabinet: an experimental investigation. Appl Therm Eng 2015;75:770–8. https://doi.org/10.1016/j.applthermaleng.2014.10.028.

[5] Ben-Abdallah R, Leducq D, Hoang HM, Fournaison L, Pateau O, Ballot-Miguet B, et al. Experimental investigation of the use of PCM in an open display cabinet for energy management purposes. Energy Convers Manage 2019;198. https://doi.org/10.1016/j.enconman.2019.111909.

[6] Ben-Abdallah R, Leducq D, Delahaye A, Fournaison L, Pateau O, Ballot-Miguet B, et al. Analysis of phase change material integration in retail display cabinets for energy management. Appl Therm Eng 2021;187:116459. https://doi.org/10.1016/j.applthermaleng.2020.116459.

[7] Rivera DR, Moraga NO. Energy analysis of convective freezer cabinet with PCMs and salmon-fillet during charging, discharging and normal operation processes by CFD modeling. J Energy Storage 2024;83:110558. https://doi.org/10.1016/j.est.2024.110558.

[8] Purohit N, Dasgupta MS. Thermal storage material enhanced refrigerated display cabinet. Mater Today Proc 2020;28:510–4. https://doi.org/10.1016/j.matpr.2019.12.210.

[9] Rocha TTM, Teggar M, Trevizoli PV, de Oliveira RN. Potential of latent thermal energy storage for performance improvement in small-scale refrigeration units: a review. Renew Sustain Energy Rev 2023;187:113746. https://doi.org/10.1016/j.rser.2023.113746.

[10] Leungtongkum T, Flick D, Hoang HM, Steven D, Delahaye A, Laguerre O. Insulated box and refrigerated equipment with PCM for food preservation: state of the art. J Food Eng 2022;317. https://doi.org/10.1016/j.jfoodeng.2021.110874.

[11] Javeri-Shahreza I, Fakhroleslam M, Sadrameli SM. Application of phase change materials for performance enhancement of open-display supermarket refrigerators: Numerical simulation and parametric study. J Energy Storage 2023;66:107506. https://doi.org/10.1016/j.est.2023.107506.

[12] Yilmaz D, Mancuhan E, Yılmaz B. Experimental investigation of PCM location in a commercial display cabinet cooled by a transcritical CO2 system. Int J Refrig 2020;120:396–405. https://doi.org/10.1016/j.ijrefrig.2020.09.006.

[13] Dhumane R, Mallow A, Qiao Y, Gluesenkamp KR, Graham S, Ling J, et al. Enhancing the thermosiphon-driven discharge of a latent heat thermal storage system used in a personal cooling device. Int J Refrig 2018;88:599–613. https://doi.org/10.1016/j.ijrefrig.2018.02.005.

[14] Qiao Y, Du Y, Muehlbauer J, Hwang Y, Radermacher R. Experimental study of enhanced PCM exchangers applied in a thermal energy storage system for personal cooling. Int J Refrig 2019;102:22–34. https://doi.org/10.1016/j.ijrefrig.2019.03.006.

[15] Liu W, Chen C, Cao J, Wu L, Ren W, Jiao D, et al. Experimental study of a novel cool-storage refrigerator with controllable two-phase loop thermosyphon. Int J Refrig 2021;129:32–42. https://doi.org/10.1016/j.ijrefrig.2021.04.009.

[16] Yuan P, Liu AL, He ZY, Chen SL, Lu YL, Sun HC, et al. Experiment and theoretical analysis of using natural cold source and cold storage in food refrigerated display cabinet. Int J Thermofluids 2024;21:100533. https://doi.org/10.1016/j.ijft.2023.100533.

[17] Yedmel MA, Hunlede R, Lacour S, Alvarez G, Delahaye A, Leducq D. A novel approach combining thermosiphon and phase change materials (PCM) for cold energy storage in cooling systems: a proof of concept. Int J Refrig 2024;158:393–404. https://doi.org/10.1016/j.ijrefrig.2023.12.015.

[18] M.A. Yedmel, R. Hunlede, S.O.L. Lacour, G. Alvarez, A. Delahaye, D. Leducq. (2023, August 21-25). A novel approach to integrate cold energy storage in a vapour compression cycle. Paper presented at the Proceedings of the 26th IIR International Congress of Refrigeration, Paris , France. doi: 10.18462/iir.icr.2023.0467.

[19] Lee S, Kang H, Kim Y. Performance optimization of a hybrid cooler combining vapor compression and natural circulation cycles. Int J Refrig 2009;32(5):800–8. https://doi.org/10.1016/j.ijrefrig.2008.12.008.

[20] Zhang H, Shi Z, Liu K, Shao S, Jin T, Tian C. Experimental and numerical investigation on a CO2 loop thermosyphon for free cooling of data centers. Appl Therm Eng 2017;111:1083–90. https://doi.org/10.1016/j.applthermaleng.2016.10.029.

[21] P. Singh. (2025). Calculateur d'humidité absolue. Retrieved from https://www.omnicalculator.com/fr/physique/calculateur-humidite-absolue.

[22] Alzuwaid FA, Ge YT, Tassou SA, Sun J. The novel use of phase change materials in an open type refrigerated display cabinet: a theoretical investigation. Applied Energy 2016;180:76–85. https://doi.org/10.1016/j.apenergy.2016.07.088.

[23] B. FRICKE, B. BECKER. (2010 of Conference). Energy Use of Doored and Open Vertical Refrigerated Display Cases. Paper presented at the International Refrigeration and Air Conditioning Conference, Purdue University. doi:http://docs.lib.purdue.edu/iracc/1154.

[24] ANSI/ASHRAE. (2005). Standard 72-2005. Method of Testing Commercial Refrigerators and Freezers. Retrieved from https://webstore.ansi.org/preview-pages/ASHRAE/preview_ANSI+ASHRAE+Standard+72-2005.pdf?srsltid=AfmBOoosZedkOia1_osEl3jneyMTl0W36ejx-BgpDPABl–G7e1Wql5U.

[25] ISO. (2015). ISO 23953-2. Refrigerated display cabinets - Part 2: Classification, requirements and test conditions. Retrieved from https://www.iso.org/standard/62002.html.

[26] Gin B, Farid MM, Bansal PK. Effect of door opening and defrost cycle on a freezer with phase change panels. Energy Convers Manage 2010;51(12):2698–706. https://doi.org/10.1016/j.enconman.2010.06.005.

[27] Mastani Joybari M, Haghighat F, Moffat J, Sra P. Heat and cold storage using phase change materials in domestic refrigeration systems: the state-of-the-art review. Energy Build 2015;106:111–24. https://doi.org/10.1016/j.enbuild.2015.06.016.

[28] Wu X, Li W, Wang Y, Chang Z, Wang C, Ding C. Experimental investigation of the performance of cool storage shelf for vertical open refrigerated display cabinet. Int J Heat Mass Trans 2017;110:789–95. https://doi.org/10.1016/j.ijheatmasstransfer.2017.03.071.
[29] Liu M, Saman W, Bruno F. Development of a novel refrigeration system for refrigerated trucks incorporating phase change material. Appl Energy 2012;92:336–42. https://doi.org/10.1016/j.apenergy.2011.10.015.
[30] Chaomuang N, Flick D, Denis A, Laguerre O. Influence of operating conditions on the temperature performance of a closed refrigerated display cabinet. Int J Refrig 2019;103:32–41. https://doi.org/10.1016/j.ijrefrig.2019.03.031.
[31] L. EVAIN. (2017). Protocole interprofessionnel de contrôle des températures des DAOA réfrigérées au stade de leur livraison/réception. In MASA (Ed.), DGAL/SDSSA/2017-425. Paris. doi:https://info.agriculture.gouv.fr/boagri/instruction-2017-425.
[32] Azzouz K, Leducq D, Gobin D. Enhancing the performance of household refrigerators with latent heat storage: an experimental investigation. Int J Refrig 2009;32(7):1634–44. https://doi.org/10.1016/j.ijrefrig.2009.03.012.
[33] A. Foster, R. Campbell, T. Davies, J. Evans. (2015 of Conference). A novel passive defrost system for a frozen retail display cabinet with a low evaporator. Paper presented at the 24th IIR International Congress of Refrigeration, Yokohama, Japan. doi: 10.18462/iir.icr.2015.0749.
[34] P. Lütolf, M. Scherer, O. Mégel, M. Geidl, E. Vrettos. (2018 of Conference). Rebound effects of demand-response management for frequency restoration. Paper presented at the 5th IEEE International Energy Conference (ENERGYCON 2018), Limassol, Cyprus, June 3-7, 2018. doi:10.1109/ENERGYCON.2018.8398849.
[35] GlobalPetrolPrices. (2025). Electricity prices. Retrieved from https://www.globalpetrolprices.com/electricity_prices/.
[36] Ribó-Pérez D, López L, Pecondón-Tricas D, Alcazar-Ortega M. A critical review of demand response products as resource for ancillary services: international experience and policy recommendations. Energies 2021;14:846. https://doi.org/10.3390/en14040846.